Accepted Manuscript

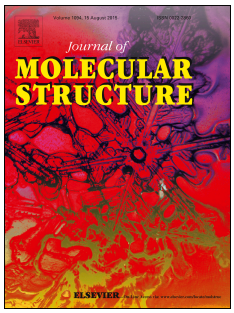

Synthesis and comprehensive structural studies of a novel amide based carboxylic acid derivative: Non–covalent interactions

Mohammad Chahkandi, Moazzam H. Bhatti, Uzma Yunus, Shahida Shaheen, Muhammad Nadeem, Muhammad Nawaz Tahir

PII: S0022-2860(16)31362-X

DOI: 10.1016/j.molstruc.2016.12.045

Reference: MOLSTR 23243

To appear in: *Journal of Molecular Structure*

Received Date: 28 October 2016

Revised Date: 14 December 2016

Accepted Date: 15 December 2016

Please cite this article as: M. Chahkandi, M.H. Bhatti, U. Yunus, S. Shaheen, M. Nadeem, M.N. Tahir, Synthesis and comprehensive structural studies of a novel amide based carboxylic acid derivative: Non–covalent interactions, *Journal of Molecular Structure* (2017), doi: 10.1016/j.molstruc.2016.12.045.

Graphical Abstract

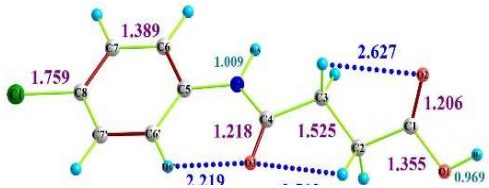

1-mon

6 ×

ΔE_{tot} = –227.59 kJ mol^{-1}

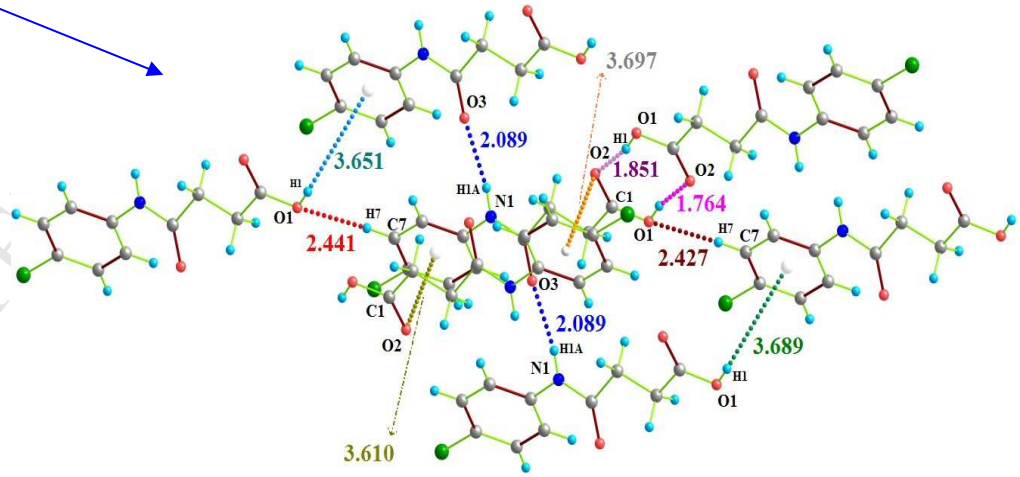

1–net

H C N O Cl

Synthesis and comprehensive structural studies of a novel amide based carboxylic acid derivative: Non–covalent interactions

Mohammad Chahkandi [a,*] Moazzam H. Bhatti [b,*], Uzma Yunus [b], Shahida Shaheen [b], Muhammad Nadeem[b], Muhammad Nawaz Tahir [c]

[a] *Department of Chemistry, Hakim Sabzevari University, Sabzevar 96179-76487, Iran.*
[b] *Department of Chemistry, Allama Iqbal Open University, Islamabad, Pakistan.*
[c] *Department of Physics, University of Sargodha,Sargodha, Pakistan.*

*To whom correspondence should be addressed:
Mohammad Chahkandi: E-mail: m.chahkandi@hsu.ac.ir; chahkandimohammad@gmail.com. Tel.: +985144013342; fax: +985144013170.
Moazzam H. Bhatti: E-mail: moazzamhussain_b@yahoo.com.

Abstract

The presented work studies the geometric and electronic structures of the crystalline network of a novel amide based carboxylic acid derivative, N–[(4–chlorophenyl)]–4–oxo–4–[oxy] butane amide, $\mathbf{C_{10}H_{10}NO_3Cl}$ (**1**), constructed *via* hydrogen bonds (HBs) and stacking non–covalent interactions. Compound **1** was synthesized and characterized by FTIR, ^{1}H, and ^{13}C–NMR, and UV–Vis spectra, X–ray structural, DTA–TG, and EI–MS, analyses. DFT calculations about molecular and related network of **1** were performed at hybrid B3LYP/6–311+G (*d*, *p*) level of theory to support the experimental data. The neutral monomeric structures join together *via* inter−molecular conventional O/N−H···O and non−conventional C−H···O HBs and O−H··π and C−O·· π stacking interactions to create 2−D architecture of the network. The results of dispersion corrected density functional theory (DFT−D) calculations within the binding energy of the constructive non−covalent interactions demonstrate that HBs, especially conventional O−H···O and N−H···O, govern the network formation. The calculated electronic spectrum show five major bands in the range of 180–270 nm which confirm the experimental one within an intense band around 250 nm. These charge transfer bands result from shift of lone pair electron density of phenyl to chlorine or hydroxyl or phenyl functional groups that possess $\pi \rightarrow \pi^*$ and $\pi \rightarrow$ n characters.

Keywords: N–[(4–chlorophenyl)]–4–oxo–4–[oxy] butane amide; Binding energy of non−covalent interaction; DFT−D; electronic transition.

1. INTRODUCTION

The amide functionality is a common feature in small or complex synthetic or natural molecules. It is universal in life, as proteins play a vital role in virtually all biological processes such as enzymatic catalysis (nearly all known enzymes are proteins), transport/storage (hemoglobin), immune protection (antibodies) and mechanical support (collagen).

Crystal engineering through control of intra–molecular interactions especially non–covalent ones, try to design of new solid network include of desired chemical and physical properties [1]. They are H–bonding, stacking, van der Waals [2], dipole–dipole [3], and more recently the halogen bond [4] which form the basis for designing of supramolecular architecture and related crystalline network [5]. The strength of halogen bond is intermediate between the strong (O–H…O) and weak (C–H…O) hydrogen bonds (HBs). It can be said that among all of them HB is more effective in control of the structure, properties and dynamics of chemical and living systems [6]. The structure of molecules can define using Bader's theory called Quantum Theory of Atoms In Molecules (QTAIM) [7]. This theory has been successfully applied to study of covalent and non–covalent atom–atom interactions in metal complexes [8], molecular clusters [9], proteins [10], and so on.

The non–covalent proteasome inhibitors, constructing different moderate inter–molecular HBs even if less widely investigated because of their potential advantages such as improved selectivity, moderate reactivity, reduced instability, and the lack of all drawbacks and side–effects might be a promising alternative to employ in therapy [5]. Some compounds including amide functional groups reported as the novel non–covalent inhibitors [6, 11-13]. In the presented new amide compound, strong O–H…O and N–H…O HBs form the pertinent network (see section 3.4.) that can facilitate the H–bonding and charge transfer (CT) interactions with acceptor molecules like DNA. In supramolecular catalyst, ligand, metal, organo–catalyst, substrate, additive, and metal counterion are reaction partners that can be held together by the non–covalent interactions [14]. Moreover, many of the inorganic–organic hybrid compounds with interesting electro–conductive, optical and magnetic properties formed using HBs [15, 16]. However, molecular functionalities, e.g. amino, amid, hydroxyl, carbonyl, and carboxylate play key role in adjusting of the fragments and following in formation of supramolecular synthons [11-13].

An in–depth analysis of the Comprehensive Medicinal Chemistry (CMC) database revealed that the carboxamide group appears in more than 25% of the known drugs [17].

There is evidence that amides, of dicarboxylic acid like maleic, succinic, and phthalic acids, containing compounds obtained by acylating of certain heterocyclic amines with the corresponding acid anhydrides, possess hypo and hypertensive, hypo and hyperglycemic, analgesic, anti–inflammatory, and anti-bacterial properties [18]. For the drug loading capacity it can be exampled that, to increase drug loading level, using the HBs of carbonyl group in doxorubicin (an amphiphilic anticancer drug), urea functional groups were built into the core of polymeric micelles [19]. Atorvastatin, the top selling drug worldwide since 2003, blocks the production of cholesterol and contains an amide bond as do Lisinopril (inhibitor of angiotensin converting enzyme), Valsartan (blockade of angiotensin–Receptors) and Diltiazem (calcium channel blocker used in the treatment of angina and hypertension. Different types of amides can be synthesized by acylation of the corresponding amines and phenyl acetic acid with maleic anhydride under mild conditions [20]. Amide bonds are typically synthesized from the union of carboxylic acid and amines. The carboxylic acid can be activated as acyl halides, acyl azide, ester, anhydride etc. There are different ways of coupling reactive carboxyl derivatives with amines [21]. The choice of coupling reagent is however critical. Our main aim was to synthesis ligand (amide bond) which have both amide and carboxylate groups as potential donor sites, for this purpose the best selection is anhydride, as anhydride readily react with vast range of nucleophiles such as alcohols, thiols amines and aromatic amine. The anhydride is succinic and chloroaniline as aromatic amine along with ethyl acetate as solvent.

Computational results as a complementary to experimental ones can help to determine the stabilized molecular and network structures, their binding and stabilization energy, vibrational frequencies of intermolecular interactions, potential energy and free energy surfaces. Beside of applying theoretical methods, Density Functional Theory (DFT) calculations provide significant results in studying of different organic and inorganic clusters at a relatively low computational cost compared with other post-Hartree-Fock methods [22-25].

In this paper we are reporting the synthesis, characterization, crystal structural, and DFT calculations of a novel amide based carboxylic acid derivative, N–[(4–chlorophenyl)]–4–oxo–4–[oxy] butane amide, $\mathbf{C_{10}H_{10}NO_3Cl}$ (**1**). DFT/B3LYP/6–311 + G(*d*, *p*) methods performed to determine the free energy of **1** and stabilization energy of the related network constructed *via* the most important non–covalent interactions. Vibrational, electronic transition assignments, frontier molecular orbital (FMO) analysis, and ^{1}H, ^{13}C, and ^{15}N–NMR chemical shifts of **1** in the ground state have been calculated. Since non–covalent

interactions play basic role for constructing the respective crystal networks, understanding this matter would be useful for designing new desired compounds.

2. Experimental

2.1. Materials and measurements

All chemicals used in this work were analytical A.R grade. FTIR spectra were recorded on thermo Scientific Nicolet iS10 spectrophotometer in ATR mode (4000–400 cm^{-1}) in KBr discs for the free ligands and all the prepared compounds. Melting points were determined via Gallenkamp (UK) 50 Hz220/240 volt melting point apparatus. The ^{1}H and ^{13}C–NMR spectrum were recorded at room temperature in DMSO on a Bruker Avance Digital 300 MHz spectrometer (Switzerland) respectively. Chemical shifts are given in ppm and coupling constant (*J*) values are given in Hz. The multiplicities of signalling are given with chemical shifts; (s = singlet, d = doublet, t, triplet, dd = doublet of a doublet). The EI–MS was performed on JEOL MS 600H–1. Thermal decomposition patterns (TG and DTA) of compound was carried out under nitrogen atmosphere up to 800°C utilizing a heating rate of 10°C/min on a DTG–60H Simultaneous DTA–TG analyzer.

2.2. Experimental procedure for the synthesis of compound 1

The independently prepared ethyl acetate solutions of 4–chloroaniline (2.5 mmol) and succinic anhydride (2.5 mmol) were mixed together drop wise. The white precipitates were appeared spontaneously after mixing. The mixture was stirred at room temperature for next 6 hours and left for overnight (Scheme 1). The precipitates were filtered, washed first by HCl (to remove unreacted aniline) and then with distilled water (to remove the unreacted succinic acid and succinic anhydride). The air dried precipitates were dissolved in acetone and set aside for recrystallization. After four weeks, needle–like white single crystals were obtained.

Yield: 43%: M.p. 178°C: Mol. Wt.: 227.1: IR (cm^{-1}): 3296 ν(OH); 3182 ν (NH); 1695 ν (carboxylic C=O); 1662 ν (ν (C=O) amide); 821 ν (ν (P–substituted stretch of benzene); ^{1}H NMR (DMSO–d_6, 300 MHz) δ(ppm): 12.11 (s,1H; OH); 10.1 (s, 1HNH); 7.62 (d, 2H, H6,6', $^{3}J[^{1}H,^{1}H]$ = 8.7Hz); 7.32 (d, 2H, H7,7'8, $^{3}J[^{1}H,^{1}H]$ = 9Hz); 2.53 (t, 2H, H2, ^{3}J[1H,1H] = 7.5 Hz); 2.52 (t, 2H, H3, ^{3}J[1H,1H] = 9 Hz): ^{13}C NMR (DMSO–d_6, 75 MHz) δ(ppm): 173 (C1); 30 (C2); 28 (C3); 170 (C4); 128 (C5); 126 (C6,6'); 120 (C7,7'); 138 (C8): EI–MS, m/z(%): $[C_{10}H_{10}ClNO_3]^{+}$, 229, M+2 (29); $[C_{10}H_{10}ClNO_3]^{+}$, 227, M (80);

$[C_{10}H_9ClNO_2]^+$, 210, (4); $[C_9H_9ClNO]^+$, 182, (1.3); $[C_7H_5ClNO]^+$, 154, (3); $[C_6H_6ClN]^+$, 127, (100); $[C_6H_4Cl]^+$, 111, (3.3); $[C_4H_5O_3]^+$, 101, (18); $[C_6H_6N]^+$, 92, (8); $[C_3H_5NO_2]^+$, 73, (15); $[C_3H_3O]^+$, 55, (14); $[CHO_2]^+$, 45, (7).

2.3. Structure determination

Crystal data were collected at 150 (2) K on a Bruker Apex II CCD diffractometer. All the non–hydrogen atoms were refined using anisotropic atomic displacement parameters, and hydrogen atoms bonded to carbon were inserted at calculated positions using a riding model. Hydrogen atoms bonded to O or N was located from difference maps and their coordinates refined. SHELXS–97 was used to solve and SHELX2012 to refine the structure. The crystal data and refinement of **1** are given in Table 1. The structure of the title compound **1** is shown in Fig. 1.

2. 4. Computational details

As starting point to geometry optimization of **1** the non–hydrogen atoms were fixed at the coordinates obtained from the crystal structure and the positions of the hydrogen atoms optimized. Then the optimization of structure of the smallest independent fragment of **1** (**1**–**mon,** see Fig. 1) along with the vibrational frequencies were performed. Following this, in order to find intermolecular interactions energies, larger fragments of **1**–**mon** (**1**–**frag1** and **1**–**frag2**; **1**–**frag3** and **1**–**frag4** containing a three and two monomer units, respectively see Fig. 1) and the final network (**1**–**net**, see Fig. 2) containing 6 monomer units and bearing all possible non–covalent interactions were optimized. All fragments were performed in the framework of the DFT method using a hybrid functional B3LYP [26–28] and the triple—ζ 6–311+G(*d*, *p*) basis set. The interaction energies were corrected for the basis set superposition error (BSSE) using the Boys–Bernardi counterpoise technique [29]. In order to take into account dispersion effects, the B3LYP–D [30] functional was used in the dispersion–corrected DFT method. The calculated vibrational frequencies indicated that the structure was stable (no imaginary frequencies). The resulting non–covalent interaction energies and related equilibrium distances and angles of the experimental and optimized network have been summarized in Tables 2 and 3. The computed geometrical parameters of **1**–**mon** with available experimental data have been compared (see Table 4). The UV–Vis spectrum was calculated for the optimized geometry with the time–dependent DFT (TD–DFT) method. Singlet and triplet excited states were both considered; however as expected, all excitations to triplet states were prohibited. Natural bond orbital (NBO)

analyses were also performed based on the optimized geometries. Partial atomic charges were computed according to natural population analysis (NPA) [31]. The isotropic ^{1}H, ^{13}C, and ^{17}O NMR chemical shifts were computed employing the same theoretical level used for the optimization calculations. Their values were reported with respect to the absolute computed isotropic shielding values of $Si(CH_3)_4$ and H_2O (with a calculated isotropic magnetic shielding of 31.99 (^{1}H), 184.01 (^{13}C), and 322.5 (^{17}O) ppm, respectively) optimized at the same respective level used for other compounds. All calculations with fully geometry optimization have been performed with Gaussian 09 [32].

3. Results and discussion

3.1. Molecular geometric: Crystal and optimized structures

Single−crystal X−ray diffraction analysis, revealed the formation of N−[(4−chlorophenyl)]−4−oxo−4−[oxy] butane amide (**1**). The single crystal data of **1** shows that the monoclinic system of unit cell belongs to the space group *P21/n* with *a*=10.9284(7) Å, *b*= 5.0641(3) Å, *c*=18.9707(14) Å, $\alpha = \gamma = 90°$, and β= 97.280(3) Å (see more information in Table 1). Selected experimental and theoretical optimized geometrical parameters including bond lengths, bond angles, and torsion angles are listed in Tables 4. The conformation of the N−H and the C=O bonds in amide segment are anti to each other. In the side chain the amide C=O is anti to adjacent C−H bond, while carboxyl C=O is syn to adjacent to C−H bond. The bond distance N_1-C_4 is 1.349(2) Å. The carboxylate group has asymmetric bond distance O_2-C_1=1.241(3) Å representing the double bond character which is slightly higher than reported value of 1.225 (2) Å and O_1-C_1=1.275(2) Å representing the single bond character. The neutral molecular compound of **1** optimized as the asymmetric monomeric unit. However, its crystalline network constructed from the molecular units through intermolecular interactions that causes to difference of experimental and optimized structural parameters of **1** (cf. Fig. 1 and Table 4). Actually a double set of every $N_1-H_{1A}\cdots O_3$, $O_1-H_1\cdots O_2$, $C_7-H_7\cdots O_1$, and $C_1-O_1\cdots \pi_{(phenyl)}$ fix the monomer in the related fragments (**1**–**frag1** to **1**–**frag4**) and the network and prevent the structural geometry of huge changing that occurred in isolated monomeric units in the gas phase. The largest differences of experimental and calculated measured structural parameters can be highlighted as 0.7 Å for O_1–C_1 bond length, 5.3° and 4° for O_2–C_1–C_2 and C_5–N_1–H_{1A} angles, and 351° for C_5–N_1–C_4–C_3 torsion angle (cf. Table 4). In the network, formation of $O_1-H_1\cdots O_2$ hydrogen bond (HB) causes to deacreasing of O_1-H_1

from and in following deacreasing of O_1–C_1 (1.275 (Exp.) and 1.355 Å (Calc.)) bond lengths in comparison to isolated optimized monomer. Moreover, involving of monomer unit in the formation of mentiond HBs resulted in changing of mentioned bond (120.89 (Exp.) and 126.17 ° (Calc.)) and torsion (176.52 (Exp.) and 175.70 ° (Calc.)) angles. In addition, it should be noted that another driving force for the mentioned structural changing of **1**−**mon** is the formation of the intra−molecular C4–O3···Hϭ HB. Actually the carbonyl group of amide functionality turns to phenyl ring that caused the changing of C_5–N_1–C_4–C_3 torsion angle from 176.5 (Exp.) to –175.7 (Calc.) in the **1**–**mon** optimized structure (see Table 4).

3.2. Spectroscopic studies

3.2.1. Infrared spectrum

The FT−IR spectrum reveals different frequencies assigned to important functional groups of **1** (Fig. 3). The important features in the IR spectrum of **1** are stretching vibration of the N–H (Exp. 3295.8, Calc. 3615 cm^{-1}) and the intense peaks that attributed to the stretching frequencies of the C=O of acid (Exp. 1696, Calc. 1807 cm^{-1}) and amide (Exp. 1662, Calc. 1751 cm^{-1}) functionality of the compound. However, the whole FT−IR spectra peaks of synthesized and experimentally recorded spectra of similar compounds [33–36] and B3LYP/6-311G+(*d,p*) optimized of **1** show good consistency (cf. Table 5). As we know, IR spectroscopy is as powerful and sensitive tool for recognition of HB formation through stretching frequency changing of D–H···A (D: donor, A: acceptor) bond. The main changes between optimized and crystal structures, as highlighted *vide supra*, are seen for O–H, N–H, and C=O functional groups participating in formation of intra–molecular HBs (for more clarity see Table 2). Significant blue shift of υ(O–H) (Exp. 3296 and Calc. 3759 cm^{-1}), υ(N–H) (Exp. 3182 and Calc. 3615 cm^{-1}), υ(C=O, amid) (Exp. 1662 and Calc. 1751 cm^{-1}), and υ(C=O, acid) (Exp. 1695 and Calc. 1807 cm^{-1}) between crystal and optimized structures confirm the formation of the related HBs (see Tables 2, 3, and 5 and Figs. 1 and 2).

3.2.2. NMR spectra

The ^{1}H and ^{13}C–NMR spectra for the compound was recorded in DMSO utilizing as the outside standard and the information are given in the experimental section. The numbering of the compound is as indicated by that appeared in Scheme 1. The characteristic peak for the OH bond in the spectrum of the compound at 12.11 ppm (Calc. 5.8 ppm) shows the

presence of the carboxylic acid. The NH gives a singlet broad peak at 10.07 ppm (Calc. 6.43 ppm) which also shows the formation of the amide bond in the ligand. This significance difference of experimental and theoretical chemical shifts of protons of hydroxyl and amide groups reveals the formation of pertinent moderate HBs [6] (O–H···O and N–H···O) in crystalline network that deshield their mentioned protons more than of optimized structure (see section 3.4.). The aliphatic protons at positions 2 and 3 (–CH_2–CH_2–) appear as triplets at 2.53ppm (^{3}J = 7.5Hz) (Calc. 2.48 and 3.32 ppm) and 2.52 ppm (^{3}J = 9Hz) (Calc. 2.89 and 2.05 ppm), respectively. The protons at the aromatic ring gives doublets at 7.32 ppm (H7, H7, ^{3}J = 9Hz) (Calc. 7.33 and 7.5 ppm) and at 7.62 ppm (H6, H6´, ^{3}J = 8.7Hz) (Calc. 6.6 and 9.13 ppm) further confirm the structure containing p–substituted phenyl ring. The higher chemical shift of H6´ comparison with H6 in optimized structure relates to formation of C4–O3···H6´ non–conventional intra–molecular HB that deshields H6´ more than H6. The ^{1}H–NMR data is given in Table 6 (Fig. 1S (see supplementary materials.).

The most downfield singlet at 173 ppm (Calc. 179 ppm) due to carbonyls (C=O) resonance for carboxylic acid at (C1) and for amide (C4) at 170 ppm (Calc. 172 ppm). The signal due to aliphatic carbons (C2 and C3) appear at 30 ppm (Calc. 29.5 ppm) and 28 ppm (Calc. 34.5 ppm) while for (C5) and (C8) signal appear at 128 ppm (Calc. 143.6 ppm) and 138 ppm (Calc. 142.5 ppm), respectively. The obtained results show that carbons participating in HBs or bond to more electronegative elements of nitrogen and chlorine became more deshielded. However the signals for phenyl carbons (C6, C6´) and C7, C7´) appeared in their respective regions, i.e., at 126 ppm (Calc. 120 and 124 ppm) and 120 ppm (Calc. 133 and 135 ppm). All these values are in agreement with each other confirm the structure of the ligand. The ^{13}C–NMR data of the ligand was in agreement with the ^{1}H–NMR and FT–IR data for the formation of ligand. The ^{13}C–NMR data is given in Table 7 (Fig. 2S (see supplementary materials.). It could be expected that the localization of excess electrons on the acceptor group and deficiency of electrons of the donor group cause to increasing the positive charge of proton because of deshilding and following promotion of the related HB. Therefore, there are lesser electron density on oxygens of carbonyl (–0.607, –0.625) (as acceptor involving in C3–H···O2 and C6´–H···O3 intra–molecular HBs) than oxygen of hydroxyl (–0.692) (as donor). However, signals of ^{17}O–NMR of O2 (Calc. 414 ppm) and O3 (Calc. 419 ppm) as HB donor and O1 (Calc. 204 ppm) as HB acceptor confirm more deshielding of two first ones.

3.2.3. Electronic spectrum

The experimental electronic spectrum of **1** includes one absorption band around 180–270 nm with a maximum at 250 nm (Fig. 4 (a)). However, the B3LYP/6–311+G (*d*, *p*) calculated UV spectrum shows six major peaks in that range at 261.5, 248.3, 204.2, 199.5, 190.7, and 189.2 nm (see Fig. 4 and Table 8). The maximum at 250 nm of the wide experimental peak recorded at 180–270 nm band could assigned with the intense calculated band at 248.3 nm. It can be concluded that the experimental and theoretical electronic spectra of **1** are consistent with each other (cf. Fig.4 and Table 8). In order to study the experimental UV spectrum and the electronic property of **1**, we need to employ the calculations of natural population analyses (NPA) of molecular orbital (MO) *via* considering its optimized ground state geometry. The optimized structure has 59 occupied MOs within singlet electron multiplicity. In followings, the constitution of FMOs that involve in CT will be discussed that all of them are organized of *s* and/or *p* and/or *d* atomic orbitals. The first and second mentioned calculated bands at 261.5 and 248.3 nm could assigned to the CT from 59 (HOMO) to 61 (LUMO+1), and 60 (LUMO), respectively. The 59 (HOMO), 60 (LUMO), and 61 (LUMO+1) consist primarily π bonding electrons of phenyl ring, empty atomic orbital of chlorine (comprising *p* 51.3% *d* 48.7%), and empty atomic orbitals of carbons of phenyl ring (*p* 71.12% *d* 28.88%) with π* character. The third calculated band at 204.2 nm is assigned to the transition from 58 (HOMO–1) to 60 (LUMO). The 58 (HOMO–1) consist primarily of π bonding electrons of phenyl ring. According to Fig. 5 the first three electronic transitions (ET) (261.5, 248.3, and 204.2 nm) belong to phenyl → chlorine/phenyl and assigned to π → π*. The fourth band of calculated electronic spectrum at 199.5 nm is attributed to CT from 58 (HOMO–1) to 60 (LUMO) and from 59 (HOMO) to 66 (LUMO+6). The 66 (LUMO+6) consist primarily of empty atomic orbital of O_1 of hydroxyl group (comprising *s* 4.42% *p* 87.8% *d* 7.8%). Therefore, this ET belongs to amide → chlorine/hydroxyl and attributed to π → π* and π → n. The fifth calculated band at 190.7 nm is related to the electronic transition from 57 (HOMO–2) to 63 (LUMO+3). The 57 (HOMO–2) and 63 (LUMO+3) consist primarily of lone pair (s) electrons of atomic orbital of O_3 of amide (comprising *s 58% p 42%*) and empty atomic orbital of chlorine (comprising *s* 19.39% *p* 87.78% *d* 7.8%). This electronic transition belongs to amide → chlorine and assigned to n → π*. The last band of the calculated UV spectrum at 189.2 nm is assigned to CT from 58 (HOMO–1) to 61 (LUMO+1). Therefore, this ET belongs to amide → phenyl and attributed to n → π* (for all transitions see Fig. 5).

3.2.4. EI-MS spectrometry

Electron impact ionization (EIMS) method was used to obtain the mass spectral data for the compound. The data are given in the experimental section along with m/z and % intensity. The resultant fragments are in good agreement with the expected structures of the compounds. In the mass spectrum molecular ion peak presented in Fig. 3S (see Supplementary materials) at m/z = 227.1 show the molecular mass of compound which is in excellent agreement with formula mass of the ligand. The [M+2] peak shows the presence of chlorine in the molecule, the base peak appear at m/z=127. The fragments are observed at m/z(%): $[C_{10}H_{10}ClNO_3]^+$, 229, M+2 (29); $[C_{10}H_{10}ClNO_3]^+$, 227, M (80); $[C_{10}H_9ClNO_2]^+$, 210, (4); $[C_9H_9ClNO]^+$, 182, (1.3); $[C_7H_5ClNO]^+$, 154, (3); $[C_6H_6ClN]^+$, 127, (100); $[C_6H_4Cl]^+$, 111, (3.3); $[C_4H_5O_3]^+$, 101, (18); $[C_6H_6N]^+$, 92, (8); $[C_3H_5NO_2]^+$, 73, (15); $[C_3H_3O]^+$, 55, (14); $[CHO_2]^+$, 45, (7) confirmed the formation of this compound.

3.3. TG–DTA analysis

The thermal analyses does not show any weight loss up to 160°C indicating the absence of any coordinated or lattice water molecules in the ligand. Its thermal degradation occurred in two steps endothermally. These two steps in the range of temperature 165–200°C & 201-305°C showed the decomposition of **1**. These two stages are in connection with a weight loss of 99%. The calculated weight loss value in these two stages is 100%. These results show good agreement with the theoretical values of total loss. The thermo analytical data are summarized in Table 9 (Fig. 4S).

3.4. DFT study of the network constructed by non-covalent interactions

The non–covalent bonds like HBs and stacking interactions hold the monomers together that stabilize the finally formed crystalline network. Herein, the binding energy of non−covalent interactions and stabilization energies of the constructed fragments and network have been fully studied. For this purpose a successful method [14, 37] explained below: First of all, the smallest independent part of CIF of **1** selected as monomer (**1–mon**) and then optimized at B3LYP/6–311+G (*d*, *p*) method. In following, using DFT–D calculations the optimization of bigger fragments (**1–frag1** to **1–frag4**) and the pertinent network (**1–net**) determine the binding energies of the involving non–covalent interactions (see Figs. 1 and 2). In the optimized and crystalline network of **1**, conventional and non–conventional HBs N−H···O and C−H···O, and unusual ∈O···π stacking contacts govern their formation. The optimized structure of **1–mon**, with structural changing related to the experimental structure, stabilized as −48.95 kJ mol^{-1} through the intra–molecular

HBs C−H···O (C_6'−H_6'···O_3 and C_2−H_{2A}···O_3). Actually, because of the larger number and more stranger of every HB than stacking one, the conventional HB govern the formation of fragments and especially the network (see Table 2 and Figs. 1 and 2). For the first equation (ΔE_1), one double set of N_1−H_{1A}···O_3 (2.126Å) and C_6'−H_{6A}'···O_3 (2.305Å) stabilize the **1–frag1** trimmer as –146.54 kJ mol^{-1}. The second trimmer fragment, **1–frag2**, stabilize through a double set of C_7−H_7···O_1 (2.452Å) as ΔE_1 = –40.22 kJ mol^{-1}. For the third and fourth equations (ΔE_3 and ΔE_4), one double set of every O_1−H_1···O_2 (1.787Å) and C_1−O_2··$\pi_{(phenyl)}$ (3.598 Å) stabilize the **1−frag3** and **1−frag4** dimmers as –99.06 and –32.60 kJ mol^{-1}, respectively. Finally, the related network **1−net** containing 7 monomers stabilized *via* all the mentioned non−covalent interactions and the interplay effects of them. There are a set of double N_1−H_{1A}···O_3 (2.089Å), a bond of every C_7−H_7···O_1 (2.427Å), O_1−H_1···O_2 (1.764Å), C_7−H_7···O_1 (2.441Å), O_1−H_1··$\pi_{(phenyl)}$ (3.651 Å), O_1−H_1··$\pi_{(phenyl)}$ (3.689Å), O_1−H_1···O_2 (1.851Å), C_1−O_2··$\pi_{(phenyl)}$ (3.697Å), and C_1−O_2··$\pi_{(phenyl)}$ (3.610 Å) that generally stabilize the network as ΔE_{tot} = –277.59 kJ mol^{-1}. They are a weak π··π interactions between the oxygen atom (O_2) of carbonyl group and the centroid of phenyl ring that reflects a weak interaction of the delocalized charge density of N atoms of the triazolo ring with the π cloud of the phenyl ring and *vice versa* (a strong interaction should be identified with a separation distance below 3.03 Å) [38]. The calculated negative of network formation energy (nfe) ($E_{nfe} = E_{network} - nE_{monomer}$) indicates that its constructed structure stabilized via non−covalent interactions. It should be pointed out that interplay effects of different D−A sites involving in HBs result in reinforcement or weakening of them. Three kinds of interplay effects could be categorized. In type A, one atom participates as Lewis acid and base in two HBs, simultaneously that resulting in reinforcement of both of them. If one atom acts as a Lewis acid (donor) or a base (acceptor) in two or three HBs simultaneously, all of them weak each other (types B and C, see Scheme 2) [14, 25b, 37]. However, there are different interplay effects of involving non−covalent interactions in the presented fragments and network of **1**. In **1-frag1** there are the diminutive effect between N_1−H_{1A}···O_3 (2.103Å) and C_6'−H_{6A}'···O_3 (2.219Å) bearing O_3 atoms that participates as an acceptor sites in both HBs, caused to bond length increasing of first ones by 0.23 Å related to CIF value and 0.086 Å for the second ones related to optimized structure of **1−mon** and raising the related stabilized energy of **1−frag** around 1.70 kJ mol^{-1} (primary values in parenthesis. cf. Table 2 and Fig. 1). Also, in **1−net** because of the participating of O_2 in the same acceptor sites, the weakening effect between O_1−H_1···O_2 (1.818Å) and C_1−O_2··$\pi_{(phenyl)}$ (3.625Å), and a cooperative effect between

$C_7-H_7\cdots O_1$ (2.482Å) and $O_1-H_1\cdots\pi_{(phenyl)}$ (3.724 Å) could be found (CIF values in parenthesis. cf. Tables 2 and 3 and Fig. 2). These diminutive effects increse the bond lengths of the mentioned interactions by 0.033 and 0.072 Å and the cooperative effects deacrese them by 0.041 and 0.073 Å which generally results in raising of the network formation energy by ~ 0.5 kJ mol^{-1}. It can be pointed out that our calculated results of binding energies of non-covalent interactions especially HBs are in good agreement with other reported calculated results using QTAIM of Bader theory [39]. Accordance to calculated binding energies of non−covalent interactions (Table 2) it can be highlighted that the conventional and non−conventional N−H···O, O−H···O, and C−H···O HBs govern the **1−net** formation as they provide more than 79% of stabilization energy of the network. Finally, this below stabilization order of the involving non−covalent interactions can be concluded: $O_1-H_1\cdots O_2$ > $N_1-H_{1A}\cdots O_3$ > $C_7-H_7\cdots O_1$ > $O_1-H_1\cdots\pi_{(phenyl)}$ > $C_1-O_2\cdots\pi_{(phenyl)}$. It is attractive to say that our calculated results of binding energies of non−covalent interactions and network stabilization energies show good accordance with other theoretical and experimental measured data [14, 37, 40].

4. Conclusion

In this work, the synthesis of a novel amide based carboxylic acid derivative, N–[(4–chlorophenyl)]–4–oxo–4–[oxy] butane amide reported and its geometric and electronic structures characterized by FTIR, ^{1}H, and ^{13}C–NMR, Mass, and UV–Vis spectra, single crystal X-ray diffraction, and DTA–TG analysis. However, the DFT−B3LYP/6−311+G(*d*,*p*) optimized geometrical parameters, vibrational, and spectroscopic results show good consistency with the experimental ones. The optimized DFT–D−B3LYP/6−311+G(*d*,*p*) **1–net** bearing 7 monomer units stabilized with HBs and stacking contacts including the conventional O/N−H···O and non−conventional C−H···O and O−H··π and C−O··π. The calculation results show that conventional HBs govern the **1–net** formation somehow the below stabilization sequence of the van der Waals contacts can be concluded: O−H···O > N−H···O > C−H···O > O−H·$\pi_{(phenyl)}$ > C−O··$\pi_{(phenyl)}$. UV calculated spectrum through TD−DFT method along with NBO analyses propose that the main electronic bands could attributed to the ET from phenyl to chlorine/hydroxyl/phenyl functional groups possessing $\pi \rightarrow \pi^*$ and $\pi \rightarrow$ n molecular orbital characters.

Supplementary materials

X–ray crystallographic information file (CIF), experimentally recorded ^{1}H–and ^{13}C–NMR and EI–MS spectra and TG–DTA curves of **1**.

Acknowledgment. MCH gratefully acknowledges the financial support by the Hakim Sabzevari University, Sabzevar, Iran. UY and MHB are thankful Allama Iqbal Open University, Islamabad, Pakistan, for providing research facilities.

References

[1] Desiraju, G. R. *Crystal Engineering. The Design of Organic Solids*, Elsevier, Amsterdam.

[2] Stefane N. Costa, Valder N. Freire, Ewerton W. S. Caetano, Francisco F. Maia Jr., Carlos A. Barboza, Umberto L. Fulco, and Eudenilson L. Albuquerque, DFT Calculations with van der Waals Interactions of Hydrated Calcium Carbonate Crystals $CaCO_3 \cdot (H_2O, 6H_2O)$: Structural, Electronic, Optical, and Vibrational Properties.*J. Phys. Chem. A*, 120 (28) (2016) 5752.

[3] (a) J-J. Hao and C-S. Wang, Rapid evaluation of the interaction energies for carbohydrate-containing hydrogen-bonded complexes **via** the polarizable dipole–dipole interaction model combined with NBO or AM1 charge. RSC Adv., 5 (2015) 6452. (b) L. L.i, R. Wu, S. Guang, X. Su, H. Xu, The investigation of the hydrogen bond saturation effect during the dipole–dipole induced azobenzene supramolecular self-assembly. PCCP, 15 (2013) 20753.

[4] Metrangolo, P.; Neukirch, H.; Pillati, T.; Resnati, G. Halogen bonding based recognition processes: a world parallel to hydrogen bonding. Acc. Chem. Res. 38 (2005) 386.

[5] B. Chattopadhyay, A. K. Mukherjee, N. Narendra, H. P. Hemantha, V. V. Sureshbabu, M. Helliwell, M. Mukherjee, Supramolecular Architectures in 5,5′-Substituted Hydantoins: Crystal Structures and Hirshfeld Surface Analyses, Crys. Growth Des. 10 (2010) 4476.

[6] G. A. Jeffrey, W. Saenger, Hydrogen Bonding in Biological Structures, Springer Verlag, Berlin, 1991.

[7] R. F. W. Bader 1990. Atoms in Molecules: A Quantum Theory (Oxford: Clarendon Press).

[8] (a) N. N. Karaush, G. V. Baryshnikov, V. A. Minaeva B. F. Minaev, A DFT and QTAIM study of the novel d-block metal complexes with tetraoxa[8]circulene-based ligands. New J. Chem. 39 (2015) 7815. (b) N. N. Karaush, G. V. Baryshnikov, B. F. Minaev, Alkali and alkaline-earth metal complexes with tetraoxa[8]circulene sheet: a computational study by DFT and QTAIM methods. RSC Adv.5 (2015) 24299.

[9] R. Parthasarthi, V. Subramanian, N. Sathyamurthy, Hydrogen bonding in phenol, water,vand phenol-water clusters. J. Phys. Chem. A 109 (2005) 843.

[10] Y. Hirano, K. Takeda, K. Miki, Charge-density analysis of an iron-sulfur protein at an ultra-high resolution of 0.48 Å. Nature 534 (2016) 281.

[11] H. N. Wang, J. S. Qin, D.Y. Du, G.J. Xu, X.L. Wang, K.Z. Shao, G. Yuan, L. J. Li, Z. M. Su. A en-templated 3D coordination polymer based on H_2pzdc with macrometallocycles. Inorg. Chem. Commun. 13 (2010) 1227.

[12] T. L. Che, Q. C. Gao, W. P. Zhang, Z. X. Nan, H. X. Li, Y. G. Cai, and J. S. Zhao, Two novel coordination polymers $[Sm_2(Pzdc)_3(H_2O)]_{\mathbf{x}} \cdot 2\mathbf{x}H_2O$ and $[Nd_2(Pzdc)_3(H_2O)]\mathbf{x} \cdot 2\mathbf{x}H_2O$: Synthesis, structure, and photoluminescent properties, Russ. J. Coord. Chem, 35 (2009) 723.

[13] H. Aghabozorg, F. Manteghi, S. Sheshmani, A brief review on structural concepts of novel supramolecular proton transfer compounds and their metal complexes. J Iran Chem Soc 5 (2008) 184.

[14] (a) M. Mirzaei, H. Eshtiagh-Hosseini, M. Chahkandi, N. Alfi, A. Shokrollahi, N. Shokrollahi, A. Janiak, Comprehensive studies of non-covalent interactions within four new Cu(II) Supramolecules. CrystEngComm, 14 (2012) 8468.; (b) M. Mirzaei, H. Eshtiagh-Hosseini, M. Mohammadi Abadeh, M. Chahkandi, A. Frontera, A. Hassanpoor, Influence of accompanying anions on supramolecular assembly and coordination geometry in Hg^{II} complexes with 8-aminoquinoline: experimental and theoretical Studies. CrystEngComm, 15 (2013) 1404.; (c) H. Eshtiagh-Hosseini, M. Mirzaei, M. Biabani, V. Lippolis, M. Chahkandi, and C. Bazzicalupi, Insight into the connecting roles of interaction synthons and water clusters within different transition metal coordination compounds of pyridine-2,5-dicarboxylic acid: experimental and theoretical studies. CrystEngComm 15 (2013) 6752.

[15] H.C. Zhou, J.R. Long, O.M. Yaghi, Introduction to metal-organic frameworks. Chem. Rev. 112 (2012) 673.

[16] T.R. Cook, Y.R. Zheng, P.J. Stang, Metal-organic frameworks and self-assembled supramolecular coordination complexes: comparing and contrasting the design, synthesis, and functionality of metal-organic materials. Chem. Rev. 113 (2013) 734.

[17] A.K. Ghose, V.N. Viswanadhan, J.J. Wendoloski, A knowledge-based approach in designing combinatorial or medicinal chemistry libraries for drug discovery. 1. A qualitative and quantitative characterization of known drug databases, Journal of combinatorial chemistry, 1 (1999) 55.

[18] N. Kolotova, V. Koz'minykh, A. Dolzhenko, E. Koz'minykh, V. Kotegov, A. Godina, B.Y. Syropyatov, G. Novoselova, Substituted amides and hydrazides of dicarboxylic acids. Part 9. Pharmacological activity of the products of interaction of 2-aminopyridines and 2-

aminopyrimidine with dicarboxylic acid anhydrides, Pharmaceutical Chemistry Journal, 35 (2001) 146.

[19] Kim SH, Tan JPK, Nederberg F, Fukushima K, Colson J, Yang C, et al. Hydrogen bonding-enhanced micelle assemblies for drug delivery. Biomaterials 2010; 31:8063e71.

[20] L. Grigoryan, M. Kaldrikyan, R. Melik-Ogandzhanyan, F. Arsenyan, Synthesis and antitumor activity of 2-N-and 3-S-substituted 5-[2-(4-) benzyloxyphenyl]-1, 2, 4-triazoles and acylhydrazides, Pharmaceutical Chemistry Journal, 46 (2012) 531.

[21] C.A. Montalbetti, V. Falque, Amide bond formation and peptide coupling, Tetrahedron, 61 (2005) 10827.

[22] (a) Streit R. Bennett, David K. Geiger, Structure and Bonding in Group 14 Congeners of Ethene: DFT Calculations in the Inorganic Chemistry Laboratory. J. Chem. Educ., 82 (1) (2005) 111. (b) U. Yunus, S. Ahmed, M. Chahkandi, M. H. Bhatti, M. Nawaz Tahir, Synthesis and theoretical studies of non–covalent interactions within a newly synthesized chiral 1,2,4-triazolo[3,4-b][1,3,4]thiadiazine. J. of Mol Struct, 1130 (2016) 688.

[23] R. A. Friesner, R. B. Murphy, M. D. Beachy, M. N. Ringnalda, W. T. Pollard, B. D. Dunietz, Y. Cao, Correlated ab Initio Electronic Structure Calculations for Large Molecules. J. Phys. Chem. A103 (13) (1999) 1913.

[24] L. Rulìsek, Z.Havlas, Using DFT methods for the prediction of the structure and energetics of metal-binding sites in metalloproteins. Int. J. Quantum Chem. 91 (2003), 504.

[25] (a) M. Chahkandi, B. Madani Khoshbakht, M. Mirzaei, A theoretical study of intramolecular H–bonding and metal–ligand interactions in some complexes with bicyclic guanidine ligands. Computational and Theoretical Chemistry 1095 (2016) 36; (b) H. Eshtiagh-Hosseini, M. Chahkandi, M.R. Housaindokht, M. Mirzaei, Bromide oxidation mechanism by vanadium bromoperoxidase functional models with new tripodal amine ligands: A comprehensive theoretical calculations study. Polyhedron 60 (2013) 93.

[26] C. Lee, R.G. Parr, W. Yang, Development of the Colle-Salvetti correlation-energy formula into a functional of the electron density. Phys Rev 37 (1988) B785.

[27] A.D. Becke, Density-functional thermochemistry. III. The role of exact exchange. J Chem Phys 98 (1993) 5648.

[28] A.D. Becke, Density-functional exchange-energy approximation with correct asymptotic behavior. Phys Rev A 38(1988) 3098.

[29] S. B. Boys and F. Bernardi, The calculation of small molecular interactions by the differences of separate total energies. Some procedures with reduced errors. Mol. Phys. 19 (1970) 553.

[30] P. Jurecka, J. Cerny, P. Hobza and D. R. Salahub, Density functional theory augmented with an empirical dispersion term. Interaction energies and geometries of 80 noncovalent complexes compared with ab initio quantum mechanics calculations. J Comput Chem, 28 (2007) 555.

[31] A.E. Reed, L.A. Curtiss, F. Weinhold, Intermolecular interactions from a natural bond orbital, donor-acceptor viewpoint. Chem. Rev. 88 (1988) 899.

[32] M. J. Frisch, G. W. Trucks, et. al., GAUSSIAN09, revision A.02; Gaussian, Inc.: Wallingford, CT, 2009.

[33] S. Renuga, S. Muthu, Molecular structure, normal coordinate analysis, harmonic vibrational frequencies, NBO, HOMO-LUMO analysis and detonation properties of (S)-2-(2-oxopyrrolidin-1-yl) butanamide by density functional methods. Spectrochimica Acta Part A: Molecular and Biomolecular Spectroscopy 118 (2014) 702.

[34] A. K. Dioumaev, Mark S. Braiman, Modeling Vibrational Spectra of Amino Acid Side Chains in Proteins: The Carbonyl Stretch Frequency of Buried Carboxylic Residues. J. Am. Chem. SOC. 117 (1995) 10572.

[35] M Karakaya, M Yildiz. A study on optimum transition state and tautomeric structures of a bis-heterocyclic monoazo dye. Indian J. Phys. 89(2) (2015) 107.

[36] W. O. George, J. H. S. Green, D. Pailthorpe, The OH stretching vibrations of 2-hydroxy carboxylic acids. J. Mol. Structure, 10 (1971) 297.

[37] M. Chahkandi, Theoretical investigation of non-covalent interactions and spectroscopic properties of a new mixed-ligand Co(II) complex. J. Mol. Struct. 1111 (2016) 193.

[38] (a) T. J. Mooibroek, P. Gamez and J. Reedijk, Lone pair–π interactions: a new supramolecular bond? CrystEngComm, 10 (2008) 1501; (b) M. Egli and S. Sarkhel, Acc. Chem. Res., 40 (2007) 197.

[39] (a) G. V. Baryshnikov, B. F. Minaev, V. A. Minaeva, V. G. Nenajdenko, Single crystal architecture and absorption spectra of octathio[8]circulene and sym-tetraselenatetrathio[8]circulene: QTAIM and TD-DFT approach. J Mol Model 19 (2013) 4511. (b) B. F. Minaev, G. V. Baryshnikov, V. A. Minaeva, Electronic structure and spectral properties of the triarylamine-dithienosilole dyes for efficient organic solar cells. Dyes and Pigments 92 (2011) 531.

[40] I. Heisler, S. Meech, Low-frequency modes of aqueous alkali halide solutions: glimpsing the hydrogen bonding vibration. Science 2010, 327, 857.

[41] N. de Lima, M. Ramos. A theoretical study of the molecular structures and vibrational spectra of the $N_2O\cdots(HF)_2$. J. Mol. Struct. 2012, 1008, 29.

Captions

Table 1. Crystal data collection and structure refinement details for **1**.

Table 2. The calculated non–covalent interactions distances (Å), angles (º), and their binding energies (kJ mol^{-1}) of **1–net**.

Table 3. Selected experimental and calculated HBs for **1**.

Table 4. Selected experimental and calculated atomic distances (Å) and angles (°) for **1–mon**.

Table 5. Vibrational frequencies with X–ray structure, and B3LYP/6–311+G(*d*, *p*) optimized structures of **1**.

Table 6. Experimental ^{1}H–NMR data of **1**.

Table 7. Experimental ^{13}C–NMR data of **1**.

Table 8. Calculated and experimental electronic data for **1**.

Table 9. Thermal data of **1**.

Scheme 1. The synthetic route for the synthesis of N–[(4–chlorophenyl)]–4–oxo–4–[oxy] butane amide (**1**).

Scheme 2. Spatial arrangement of interacting fragments in assisting (Type A) and debilitating (Type B and C) HBs. D and A denote donor and acceptor sites [25b, 41].

Figure 1. ORTEP diagram of the **1** drawn at 50 % probability level. The H–atoms are drawn as small circles of arbitrary radii and B3LYP/6–311+G(*d*, *p*) Optimized structures of monomer (**1–mon**) and fragments of **1**; the equations used to evaluate the different non–covalent interactions in compound (distances are given in Å).

Figure 2. Formation energy of **1–net** from **1–mon** (distances are given in Å). The calculated stabilization energy is only relative to expansion of molecular compound to its network.

Figure 3. Experimental FTIR (cm^{-1}) spectrum for **1**.

Figure 4. Experimental electronic spectra in methanol (a) and calculated–B3LYP/6–311+G(*d*, *p*) one (b) for **1**.

Figure 5. Frontier molecular diagrams for **1** involving in CT obtained according to the B3LYP/6–311G+ (*d*, *p*).

Table 1.

Compound	1
Empirical formula	$C_{10}H_{10}ClNO_3$
Formula weight	227.64
Temperature	296(2)
Crystal system	Monoclinic
Wavelength (Å)	0.71073
Space group	P21/n (No. 14)
Unit cell dimension	
a (Å)	10.9284(7)
b (Å)	10.9284(7)
c (Å)	18.9707(14)
α (°)	90
β (°)	97.280(3)
γ (°)	90
V(Å^3)	1041.42(12)
Z	4
Crystal size (mm)	0.42 x 0.22 x 0.20
θ Range for data collection (°)	3.541 to 27.488
D calc (Mg/m^3)	1.452
Absorption coefficient(mm^{-1})	0.352
F(000)	472
Reflections collected	2386
S (goodness of fit) on F^2	1.028
Independent reflections	1718

Table 2.

	d(H···A)	< (DHA)	Binding Energy
$O_1-H_1\cdots O_2$	1.764	169.65	−50.08
$O_1-H_1\cdots O_2$	1.851	172.36	−44.61
$N_1-H_{1A}\cdots O_3$	2.089	167.70	−42.17
$C_7-H_7\cdots O_1$	2.427	160.29	−20.73
$C_7-H_7\cdots O_1$	2.441	161.14	−20.39
$O_1-H_1\cdot\cdot\pi_{(phenyl)}$	3.651	107.37	−15.16
$C_1-O_2\cdot\cdot\pi_{(phenyl)}$	3.610	94.68	−14.82
$O_1-H_1\cdot\cdot\pi_{(phenyl)}$	3.689	108.95	−14.26
$C_1-O_2\cdot\cdot\pi_{(phenyl)}$	3.697	95.09	−13.20

Stabilization Energy	Interaction Types
ΔE_1 –146.54	2 × ($N_1-H_{1A}\cdots O_3$ (*2.126 Å**), $C_6'-H_6'\cdots O_3$ (*2.305 Å**))
ΔE_2 –40.22	2 × ($C_7-H_7\cdots O_1$ (2.452 Å))
ΔE_3 –99.06	2 × ($O_1-H_1\cdots O_2$ (1.787 Å))
ΔE_4 –32.60	2 × ($C_1-O_2\cdot\cdot\pi_{(phenyl)}$ (3.598 Å))
ΔE_{tot} –277.59	2 × ($N_1-H_{1A}\cdots O_3$ (2.089 Å)) + $C_7-H_7\cdots O_1$ (2.427 Å), $O_1-H_1\cdots O_2$ (1.764 Å) + $C_7-H_7\cdots O_1$ (2.441 Å), $O_1-H_1\cdots\pi_{(phenyl)}$ (3.651 Å) + $O_1-H_1\cdots\pi_{(phenyl)}$ (3.689 Å) + $O_1-H_1\cdots O_2$ (*1.851 Å**), $C_1-O_2\cdot\cdot\pi_{(phenyl)}$ (*3.697 Å**) + $C_1-O_2\cdot\cdot\pi_{(phenyl)}$ (3.610 Å)

* *The weakened interactions by diminutive effects shown as italic form.*

* *The reinforced interactions by cooperative effects shown as underline format.*

Table 3.

D−H···A	d(D−H)	d(H···A)	d(D···A)	<(DHA)
$O_1-H_1\cdots O_2$	0.820(e), 0.833(c)	1.818(e), 1.764(c)	2.625(e), 2.589(c)	168.3(e), 172.1(c)
$N_1-H_{1A}\cdots O_3$	0.860(e), 851(c)	2.103(e), 2.089(c)	2.946(e), 2.874(c)	166.6(e), 169.0(c)
$C_7-H_7\cdots O_1$	0.930(e), 0.917(c)	2.482(e), 2.427(c)	3.365(e), 3.312(c)	158.6(e), 162.5(c)

Symmetry codes: 1+x,y,z , 1/2−x,1/2+y,1/2−z, −1+x, −1+y,z , −1−x,1−y, −z, x,2−y, −z

e: experimental, c: calculated

Table 4.

Compound 1: $C_{10}H_{10}NO_3Cl$								
	Experimental	**Calculated**		**Experimental**	**Calculated**		**Experimental**	**Calculated**
O1–C1	1.275(2)	1.355	C3–C4	1.512(3)	1.527	C6–C7–C8	119.32	119.24
O2–C1	1.241(3)	1.206	C6–C7	1.383(3)	1.389	N1–C5–C10	121.58	123.48
O3–C4	1.220(2)	1.218	C4–N1–C5	126.46(15)	129.21	C5–N1–H1A	117.00	114.94
N1–C4	1.349(2)	1.376	C1–O1–H1	109.00	107.30	N1–C4–C3	114.57(14)	113.72
N1–C5	1.413(2)	1.412	O1–C1–C2	115.38(17)	111.34	C5–N1–C4–C3	176.52	–175.70
Cl1–C8	1.743(2)	1.759	O2–C1–C2	120.89(17)	126.17	C5–N1–C4–O3	−4.77	2.63
C1–C2	1.492(3)	1.509	O1–C1–O2	123.69(17)	122.48	C2–C3–C4–O3	8.34	27.38
C2–C3	1.503(3)	1.525	C4–N1–H1A	117.00	115.82	C3–C2–C1–O1	–167.34	–172.14
O1–H1	0.820	0.969	H3A–C3–H3B	107.81	106.13	C4–N1–C5–C10	−35.58	–1.23

Table 5.

Assignments	**Calc. for 1 (B3LYP/6–311+G(*d*, *p*))**	**Exp. for 1**	**Exp. for others** [33-36]
C–O–H bend. (out of plane)	653 s	–	–
C–NH_2 bend. (out of plane)	723 vw	–	758
CH_3 bend. (in plane)	1035 m	–	1014
C–C Al. str.	1079 m	–	1090–1053
C–Cl Ar (P–substituted)	1103 s	821	1089–1096
C–O–H bend. (in plane)	1146 vs	–	–
C–N str. (N–ph)	1261 m	–	1266
CH_2 wagging	1369–1427 m-s	–	1428, 1452
CH_2 scissoring	1463, 1472 m-s	–	–
C=N str.	1547 vs	–	–
C=C & C–N str. (N–ph)	1627, 1636 m	–	1500–1600
C=O str. (amide)	1751 vs	1662	1694
C=O str. (acid)	1807 vs	1695	1730–1760
C–H Al. str.	3038–3092 w-m	2360	2910–2982
C–H Ar str.			
N–H str. (amide)	3615 m	3182	3574
O–H str.	3759 s	3296	3440–3630

The abbreviations are, Al: aliphatic, Ar: aromatic, str: stretching, bend: bending, ph: phenyl, s: strong, m: medium, w: weak, and vw: very weak.

Table 6.

Chemical shift (ppm)	Multiplicity	Integration	Proton Assignment
2.52	t, $^{3}J[^{1}H,^{1}H]$ = 9 Hz	2H	CH_2 [H2]
2.53	t, $^{3}J[^{1}H,^{1}H]$ = 7.5 Hz	2H	CH_2 [H3]
7.32	d, $^{3}J[^{1}H,^{1}H]$ = 9 Hz	2H	Ar-H[H7,7´]
7.62	d, $^{3}J[^{1}H,^{1}H]$ = 8.7 Hz	2H	Ar-H[H6,6´]
10.11	s	1H	NH
12.11	s	1H	OH

t = triplet, d = doublet, s = singlet

Table 7.

Chemical shift (ppm)	Carbon assignment
173	C1
170	C4
120	C7,C7´
126	C6,C6´
30	C2
28	C3
128	C5
138	C8

Table 8.

Exp. Wave length(nm) of **1**	**Calc. of 1 (NPA & TD-DFT)**		
	Wave Length(nm)	Oscillator strength	Assignment
180-270	261.5	0.017	59 (HOMO) → 61 (LUMO+1)
180-270	248.3	0.503	59 (HOMO) → 60 (LUMO)
180-270	204.2	0.056	58 (HOMO–1) → 60 (LUMO)
180-270	199.5	0.152	58 (HOMO–1) → 60 (LUMO) 59 (HOMO) → 66 (LUMO+6)
180-270	190.7	0.110	57 (HOMO–2) → 63 (LUMO+3)
180-270 .	189.2	0.297	58 (HOMO–1) → 61 (LUMO+1)

Table 9.

Compound	Number of Stages	Temp. range (^{o}C)	Tmax. (^{o}C) 150-380	Thermogravimetry(TG)		
				Mass Loss (%) Observed		Mass Loss (%) calculated
N-[(4-chlorophenyl)]-4-oxo-4-[oxy] butanamide	2	165-200	181 (+)	9.8		
		201-305	260 (+)	89.4	> 99	100

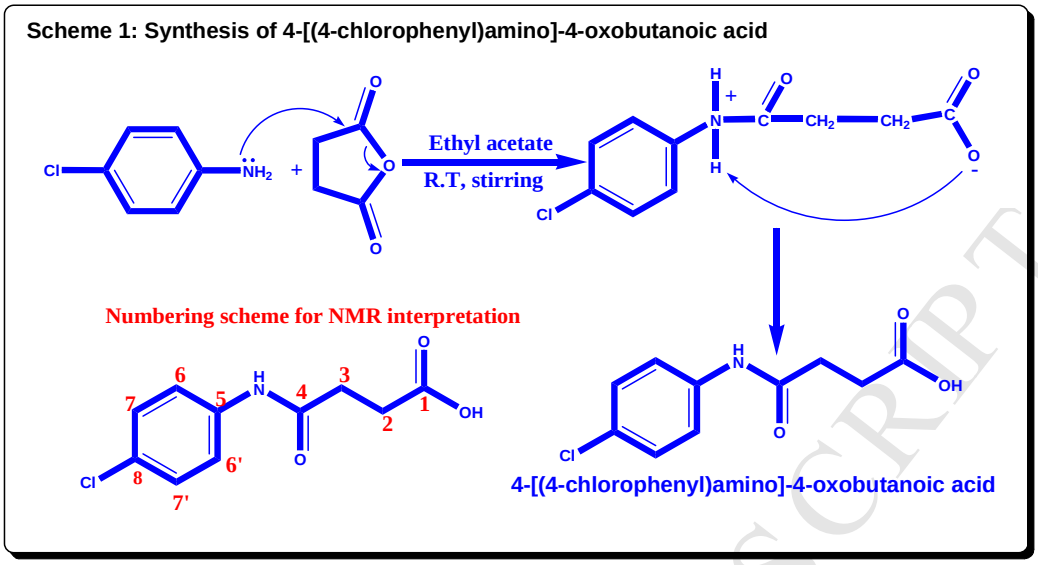

Scheme 1.

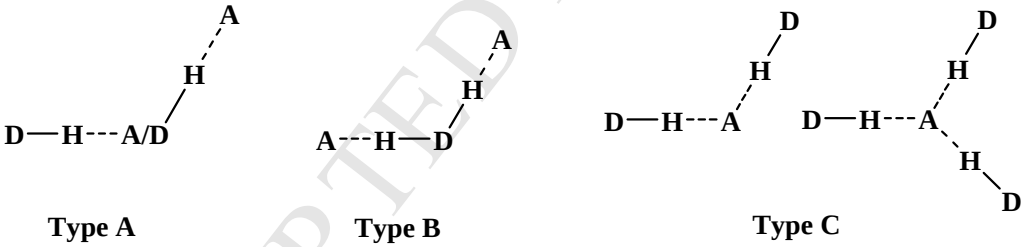

Scheme 2.

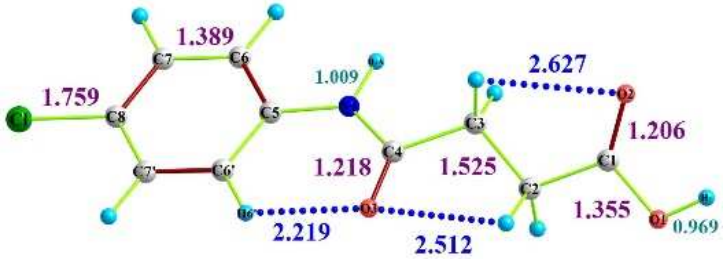

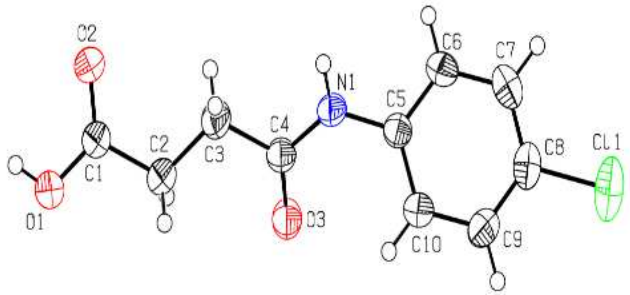

1-mon

$\Delta E_1 = -146.54$ kJ mol^{-1}

× 3

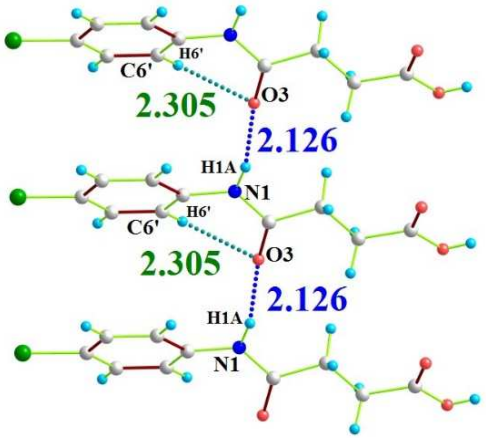

1-frag1

3 ×

$\Delta E_2 = -40.22$ kJ mol^{-1}

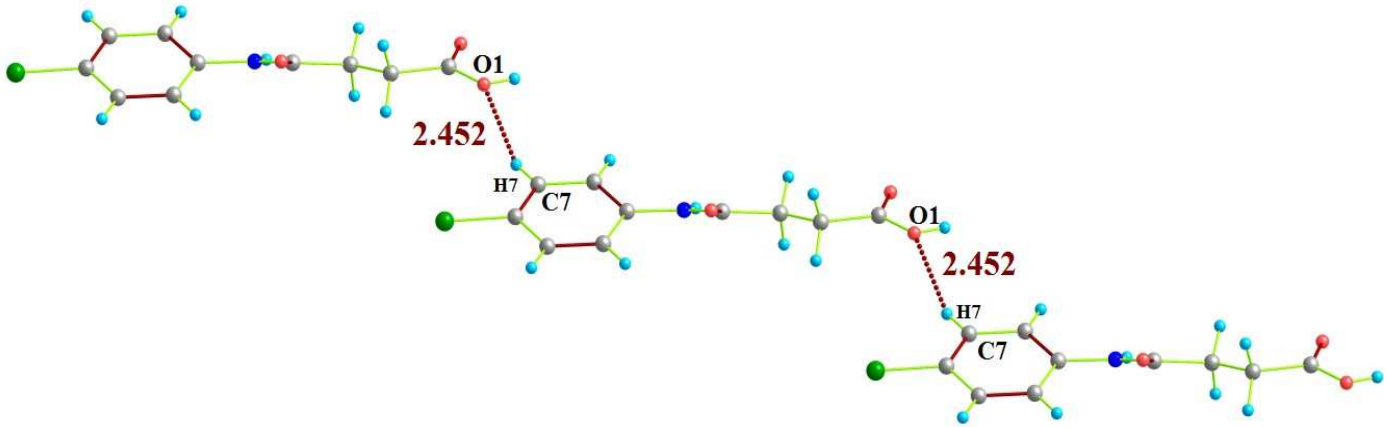

1-frag2

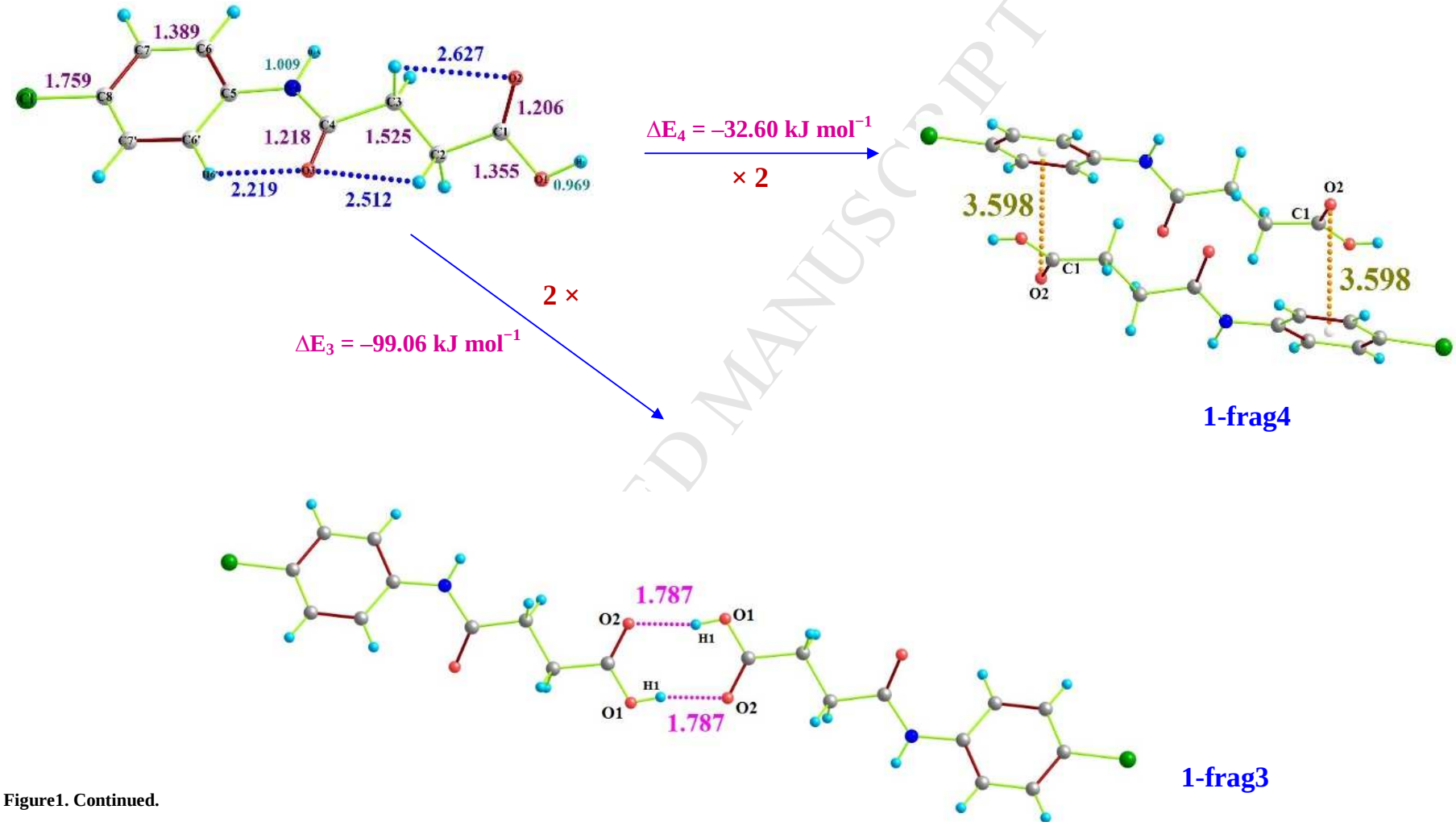

Figure1. Continued.

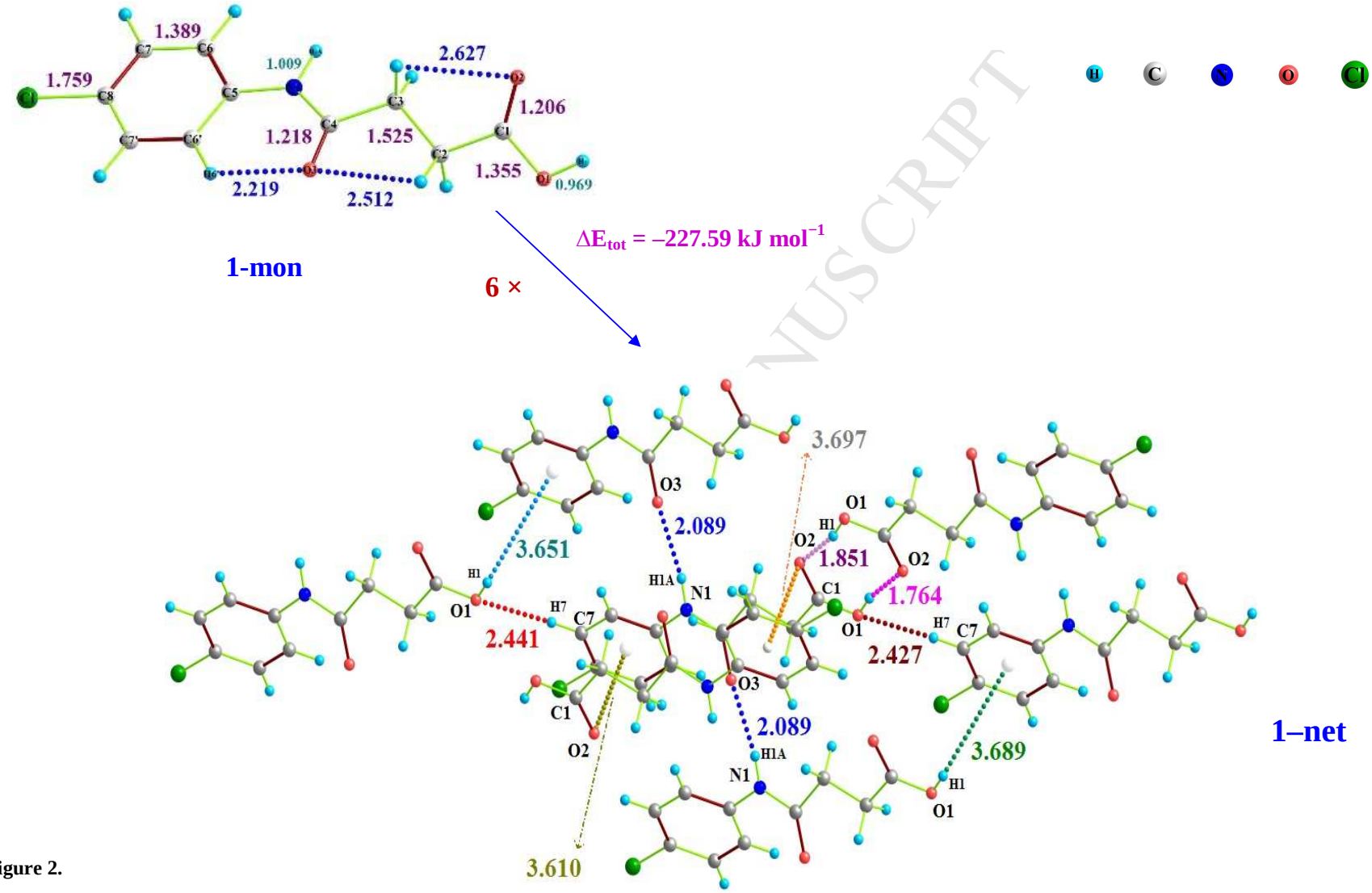
H
C
N
O
Cl
1.389
1.759
1.009
2.627
1.206
1.218
1.525
1.355
0.969
2.219
2.512
1-mon
ΔE_{tot} = –227.59 kJ mol^{-1}
6 ×
3.697
3.651
2.089
1.851
1.764
2.441
2.427
2.089
3.689
3.610
1–net

Figure 2.

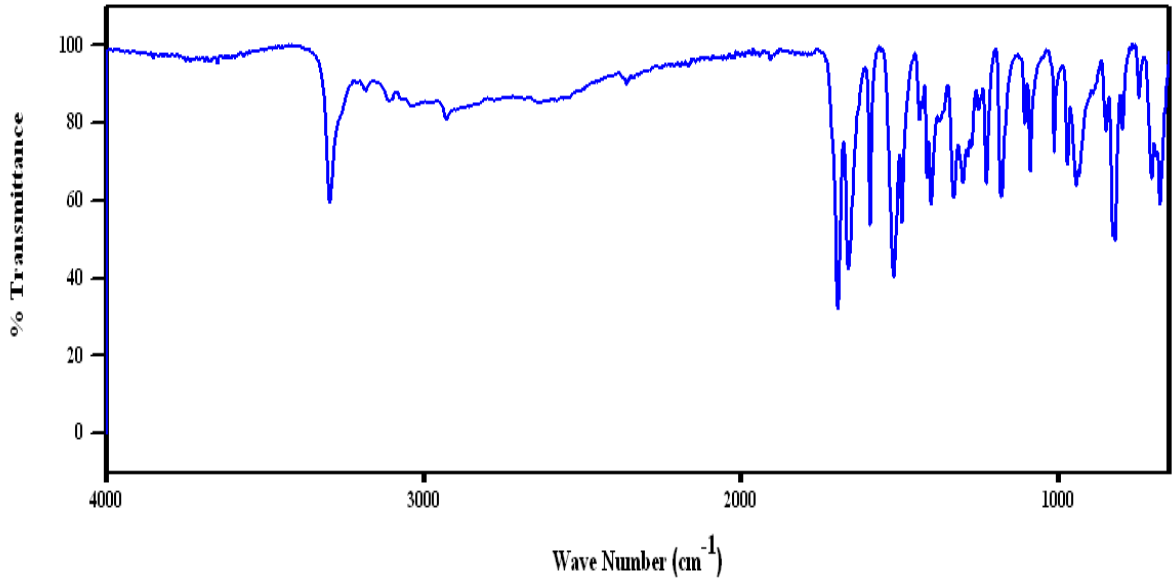

Figure 3.

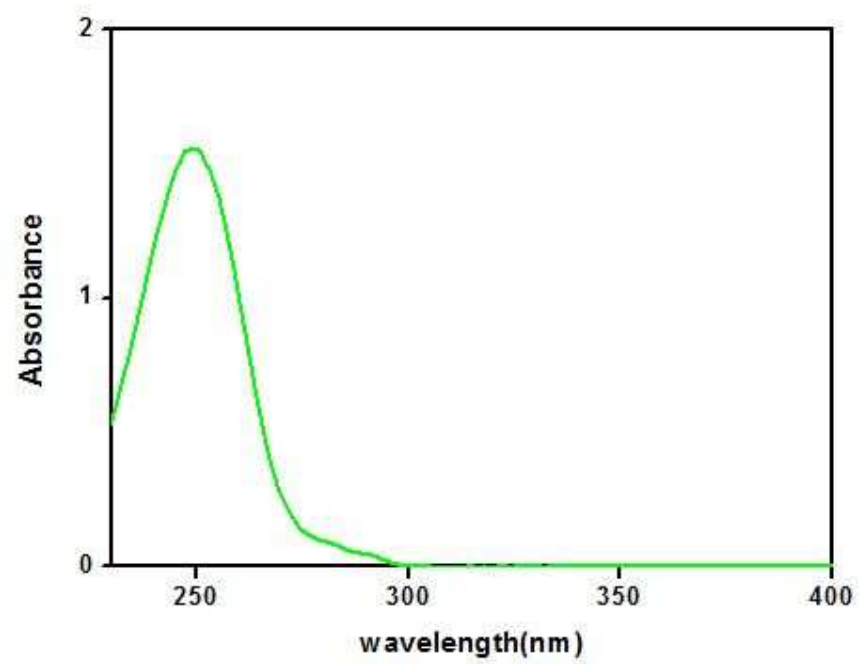
Absorbance
2
1
0
250
300
350
400
wavelength(nm)

(a)

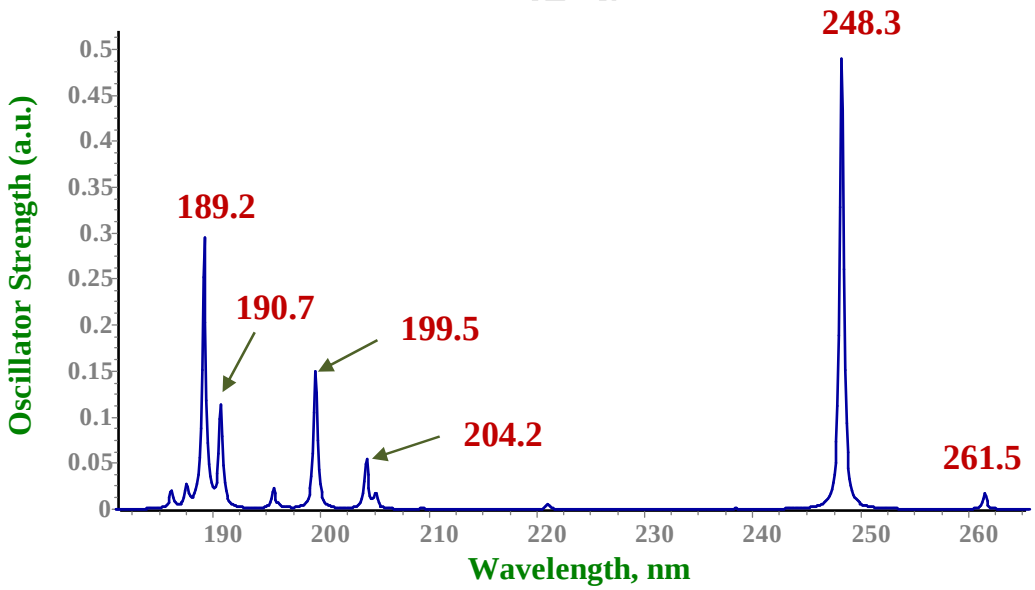
Oscillator Strength (a.u.)
0.5
0.45
0.4
0.35
0.3
0.25
0.2
0.15
0.1
0.05
0
189.2
190.7
199.5
204.2
248.3
261.5
190
200
210
220
230
240
250
260
Wavelength, nm

(b)

Figure 4.

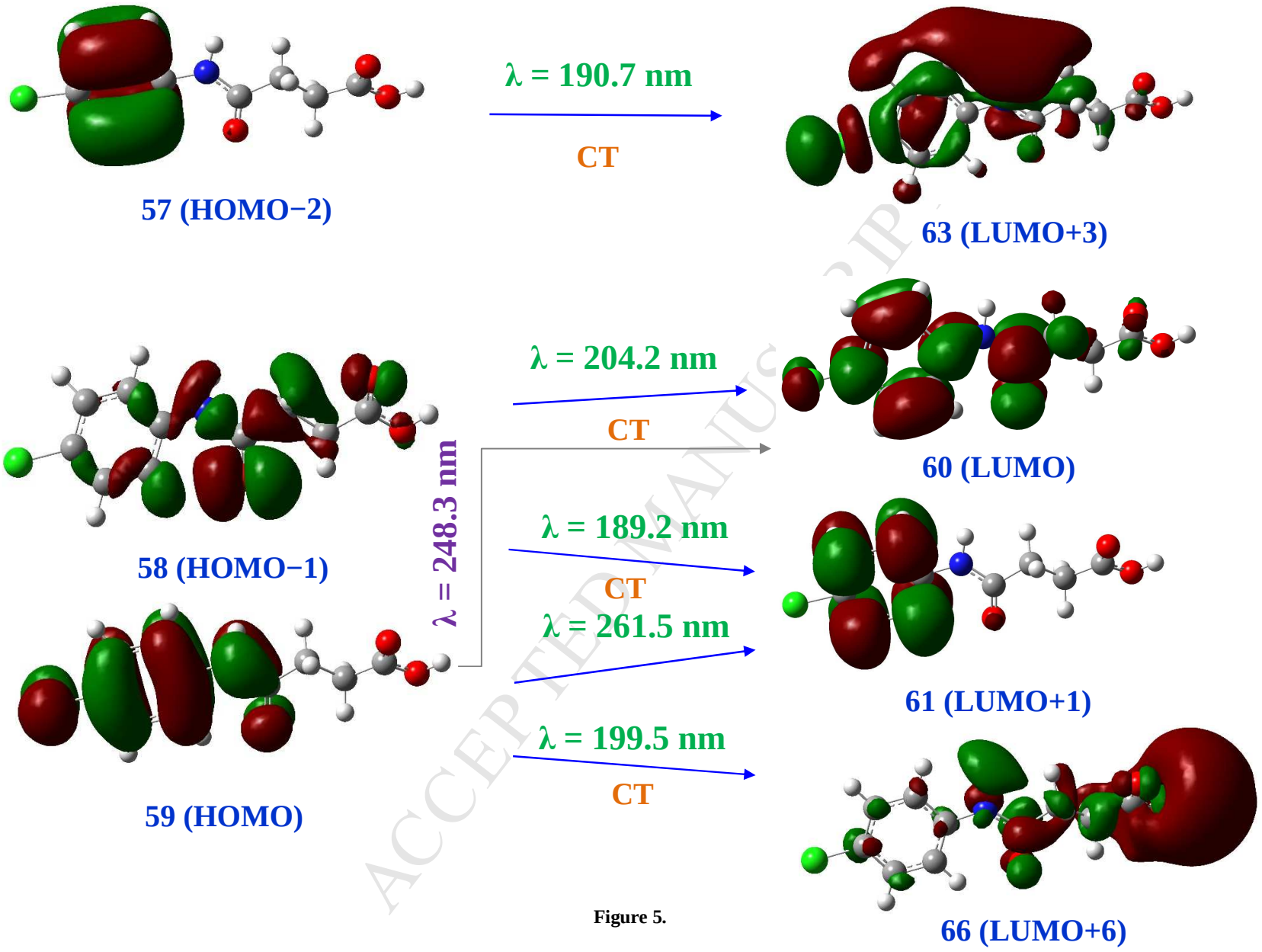
λ = 190.7 nm
CT
57 (HOMO−2)
63 (LUMO+3)
λ = 204.2 nm
CT
60 (LUMO)
58 (HOMO−1)
λ = 248.3 nm
λ = 189.2 nm
CT
λ = 261.5 nm
61 (LUMO+1)
λ = 199.5 nm
CT
59 (HOMO)
66 (LUMO+6)

Figure 5.

Highlights

- Synthesis of a novel amide based carboxylic acid derivative, **$C_{10}H_{10}NO_3Cl$** (**1**).
- Structural characterization by X-ray diffraction, and others spectroscopies.
- Study of the constructive non–covalent interactions by DFT–D calculations.
- The network stabilized by O/N−H···O, C−H···O, O−H··π, and C−O··π contacts.